## ▌ Biological Chemistry & Chemical Biology

# DNA-Binding and Anticancer Activity of Pyrene-Imidazolium Derivatives

Riccardo Bonsignore,[a] Antonietta Notaro,[a] Anna Maria Pia Salvo,[a] Angelo Spinello,[b] Giuseppe Fiasconaro,[a] Alessio Terenzi,[c, d] Francesco Giacalone,[a] Bernhard K. Keppler,[c, d] Michela Giuliano,*[a] Michelangelo Gruttadauria,*[a] and Giampaolo Barone*[a]

DNA-binding investigations showed that two different derivatives endowed with pyrene and imidazolium moieties, **1** and **2**, strongly bind both double-stranded DNA and telomeric sequences in G-quadruplex (G4) conformation. The values of the DNA-binding constants indicate that **1** and **2** show preferential affinity for G4-DNA, of about one and two orders of magnitude, respectively. Moreover, **1** and **2** inhibit short and long-term proliferation of breast cancer cell lines in a time- and dose-dependent fashion. Remarkably, senescence assays indicate that telomeric G4-DNA is a possible biotarget for the cytotoxic activity of **2**. Molecular dynamics simulations suggest that the stronger binding of **2** with G4-DNA and the related senescence induction, are a consequence of additional edge-to-face interactions with a base in the TTA loop.

## Introduction

The nature and strength of the interaction of small molecules with DNA are still considered essential information to explain the biological properties shown by a number of carcinogenic compounds as well as by new potential anticancer drugs.[1–3]

This subject has been investigated since long time and few structural features that designed small molecules must possess, to effectively interact with DNA, are nowadays well known. Restricting our interest to non-covalent interactions with DNA, the presence of polar or, better, positively charged groups is crucial for the electrostatic attraction between the small molecule and the negatively charged sugar-phosphate DNA backbone. In addition, the presence of aromatic planar groups is key to allow $\pi$-$\pi$ stacking interactions with the DNA nitrogen bases, occurring in intercalation or top stacking.[4, 5] Very often

the two groups are present in one molecule: the aromatic ring can be positively charged,[6] positively charged residues can be appended on side groups,[7,8] or a positive charge is conferred by metal ions in complexes of aromatic ligands.[9, 10]

In this context, it has been recently reported that a dicationic pyrene-imidazolium derivative, in which two pyrene-imidazolium units are bridged by a $C_1$ linker, is able to selectively bind to G-quadruplex (G4) DNA, preferring it to double-stranded (ds) DNA.[11] G4-DNA consists of short tracts of guanine-enriched sequences with the capabilities to fold into tetrads in which each guanine is linked to the other by means of Hoogsten hydrogen bonds. Each of the tetrad is stabilised both by $\pi$-$\pi$ stacking interactions and by the presence of cations (usually $K^+$) inside the channel constituted by the O6 atoms of the guanines.

G4 sequences are mainly located in human telomeres, the structures critical for the proliferation and survival of dividing cells, including cancer cells, and in oncogene promoter regions.[12] Recently, they have been also found in human cells.[13] Furthermore, it is known that G4-DNA is also involved in other regulatory processes as well as in DNA replication and mRNA translation. For example they have been found in the 5'-untranslated region of mRNA where they seem to inhibit translation.[14, 15] In the last years, great interest has been directed toward G4 binders, which are able to interfere with telomere function in different ways, for example by inhibiting telomerase activity, delocalising specific telomeric proteins, or activating DNA damage response.[14, 16] It is well known that in the most of normal cells, the absence of mechanisms of telomere elongation is responsible for their shortness to a critical length and this event leads to replicative senescence and growth arrest. Differently, it has been demonstrated that the maintenance of telomere length is fundamental for cancer cell survival and, for this reason, these structures have been proposed as possible targets of anticancer therapy.[17]

[a] Dr. R. Bonsignore, Dr. A. Notaro, Dr. A. M. P. Salvo, Dr. G. Fiasconaro, Dr. F. Giacalone, Prof. M. Giuliano, Prof. M. Gruttadauria, Prof. G. Barone
Dipartimento di Scienze e Tecnologie Biologiche Chimiche e Farmaceutiche
Università degli studi di Palermo
Viale delle Scienze, Edificio 17, 90128, and Plesso di Biochimica, Via del Vespro 129, 90127, Palermo, Italy
E-mail: michela.giuliano@unipa.it
        michelangelo.gruttadauria@unipa.it
        giampaolo.barone@unipa.it

[b] Dr. A. Spinello
CNR-IOM-Democritos National Simulation Center c/o SISSA
via Bonomea 265, 34165, Trieste, Italy

[c] Dr. A. Terenzi, Prof. B. K. Keppler
Institute of Inorganic Chemistry
University of Vienna
Waehringerstr. 42, A-1090 Vienna, Austria

[d] Dr. A. Terenzi, Prof. B. K. Keppler
Research Platform "Translational Cancer Therapy Research"
University of Vienna and Medical University of Vienna
Vienna, Austria

💻 Supporting information for this article is available on the WWW under http://dx.doi.org/10.1002/slct.201601502

Several G-quadruplex binders have been tested in the last decade, see e.g.[15,18], with one of them (Quarfloxin) entering phase II clinical trials for the treatment of neuroendocrine/carcinoid tumours,[19] unluckily with no final success due to bioavailability issues.

Pyrene-imidazolium derivatives have recently found several applications as fluorescent sensors for ATP,[20] for G-quadruplex forming DNA,[11,21] and for lanthanide ions in aqueous solutions.[22]

Starting from the promising DNA-binding properties of such class of compounds,[11] in the present manuscript we have studied the effect of the presence of an alkyl chain bridging two pyrene-imidazolium groups on their interaction with duplex and G4-DNA. In fact, the presence of a $CH_2$ unit linking two pyrene-imidazolium moieties makes such compound a selective G4-DNA binder. Interestingly, a groove binding mechanism was proposed toward both duplex and G4-DNA.[11] In particular, although in principle the two pyrene moieties may bind duplex DNA by bis-intercalation, and G4-DNA by top-stacking and groove binding, self-stacking interactions prevail and the bulkier conformation interacts with both DNA structures only by groove binding. To our knowledge, the biological properties of such kind of compounds were not yet reported in the literature.

On the other hand, a very recent approach for the selective design of G4-binders is to connect two charged binding moieties, equal or different, by flexible linkers of variable length.[23–26] Interestingly, with this approach two platinum(II) terpyridine complexes separated by flexible chains were found to bind ds- and G4-DNA by various mechanisms: major and minor groove binding with duplex DNA; top-stacking and groove binding with G4-DNA.[23]

With the aim of designing new pyrene-imidazolium derivatives with improved binding affinity and selectivity for G4-DNA, in the present work we have correlated the DNA binding properties of the title compounds with their effect on the growth of breast cancer cells. Today, breast cancer is the second leading cause of cancer-related mortality worldwide and the most common cancer among women. We employed MDA-MB231 cells, which are a highly invasive, estrogen receptor (ER) negative cell lines, and a model for triple-negative breast cancers (TNBCs) with poorer outcomes, and MCF-7 cells, ERα-positive breast carcinoma cells.

## Results and Discussion

Monocationic salt **1** (Figure 1) was prepared by reaction of 1-(bromomethyl)pyrene with 1-methylimidazole. Dicationic salt **2** (Figure 1), in which two pyrene-imidazolium units were bridged by a $C_4$ linker, was prepared by reaction of 1-(bromomethyl) pyrene with 1,1′-(1,4-butanediyl)bis(imidazole). The aim of the synthesis was to check the effect of a $C_4$ linker on the DNA-binding mechanism and on the biological properties of pyrene-imidazolium derivatives.
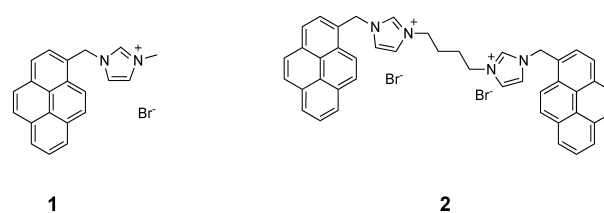


**Figure 1.** Chemical structures of compounds **1** and **2**.

## DNA binding

The DNA binding of **1** and **2** was first investigated by means of UV-vis spectroscopy, adding increasing amounts of the telomeric sequence in G4 conformation or ds-DNA (Figure 2 and
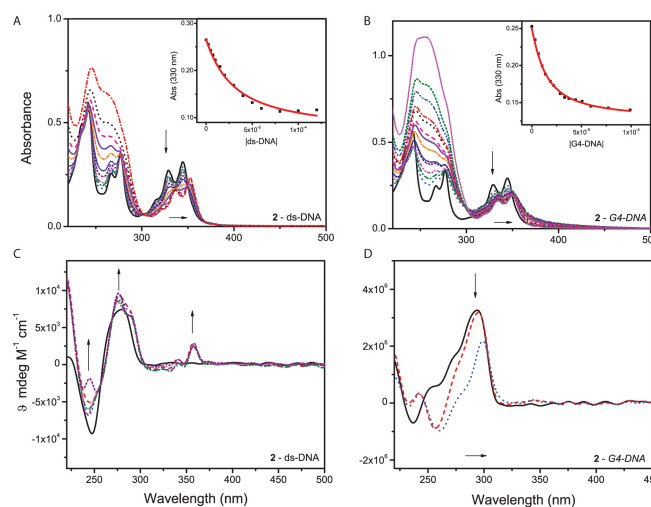


**Figure 2.** UV-vis and CD spectra of **2**-DNA solutions, collected in 100 mM KCl and 50 mM Tris-HCl buffer: (A,C) ds-DNA and (B,D) G4-DNA. A) [**2**] = 8.0 μM, [$DNA_{phosphate}$] = 0.0 – 120.0 μM; (B) [**2**] = 7.5 μM, [G4-DNA] = 0.0 – 4.5 μM; (C) [$DNA_{phosphate}$] = 49.6 μM; [**2**] = 0.0–41.3 μM; (D) [G4-DNA] = 2.2 μM, [**2**] = 0.0 – 35.0 μM. Fits used to obtain binding constants are shown in the insets. G4-DNA concentration is expressed in monomer units.

supplementary Figure S1) to solutions with fixed concentration of the two molecules. The UV-vis spectra of **1** and **2** are characterised by an intense band at about 242 nm and by weaker bands at about 265 and 275 nm. Moreover, two additional absorption bands, at about 326 and 342 nm for **1** (Figure S1) and at 330 and 344 nm for **2** (black solid lines in Figures 2A and 2B) are present in a region where DNA does not absorb.

The addition of increasing amounts of DNA drastically affects the spectra of both **1** and **2**. In particular, the bands at 326 and 342 nm of **1** and at 330 and 344 nm of **2**, are red shifted of ca. 10 nm and their intensity is drastically reduced in the presence of both ds- and G4-DNA.

The intrinsic binding constants of the compound/DNA complexes were obtained by fitting the experimental absor-

bances (Abs) at 342 nm for **1** and at 330 nm for **2**, plotted as a function of the molar concentration of duplex DNA (inset in Figures 2A and S1A) and of G4-DNA (inset in Figures 2B and S1B), as recently reported[27,28] (see ESI for further details).

The $K_b$ values obtained are reported in Table 1 and show that both molecules bind to double helical DNA with compara-

| Table 1. DNA-binding constants ($K_b$) of **1** and **2** with ds-DNA and G4-DNA. | | |
|---|---|---|
| | **1** | **2** |
| ds-DNA | $(1.3 \pm 0.1) \times 10^4$ $M^{-1}$ | $(3.8 \pm 0.5) \times 10^4$ $M^{-1}$ |
| G4-DNA | $(1.8 \pm 0.4) \times 10^5$ $M^{-1}$ | $(2.1 \pm 0.2) \times 10^6$ $M^{-1}$ |

ble affinity. Nonetheless, a tighter binding always occurs with telomeric G4-DNA, with $K_b$ values of one and two orders of magnitude larger, for **1** and **2**, respectively, than those with ds-DNA.

DNA-melting measurements confirm that compound **2** stabilizes G4-DNA more efficiently than compound **1**, with a $\Delta T$ of 4.5 and 2.9 °C, respectively (see supplementary Figure S2).

The nature of the DNA-binding of both title compounds was investigated also by recording the Circular dichroism (CD) of ds-DNA 50 μM solutions in the presence of increasing amounts of **1** (supplementary Figure S1C) and **2** (Figure 2C). The addition of **1** and **2** modifies the CD spectrum of ds-DNA, by increasing the intensity of both the positive and negative bands at 275 nm and 245 nm. Moreover, a weak induced CD band occurs at ca. 370 nm in presence of **2** (Figure 2C). These results, attributable to conformational changes in native DNA, highlight the strong binding of **1** and **2** with ds-DNA, as evidenced by the $K_b$ values. Similar spectral modifications have been in the literature essentially attributed to DNA-intercalation.[29]

The CD of telomeric G4-DNA in presence of $K^+$ ions, characterised by a strong positive band at 290 nm and a shoulder at about 270 nm, is typical of a hybrid G4 structure with mixed parallel/antiparallel strands.[30–32] The addition of **1** and **2** induces modifications to the CD of G4-DNA (Figures S1D and 2D), which are stronger in presence of **2** and attributable to a tighter binding of **2**, compared to **1**.

The emission profile of **1** (black solid lines in Figures S3A and S3B), excited at 344 nm, is characterized by the presence of three peaks at 376, 396 and 416 nm, which are related to the vibronic bands of pyrene.[33] The intensity of these bands monotonously decreases in presence of increasing amounts of duplex and G4-DNA, confirming the interaction of the derivative with the polynucleotides. Interestingly, excited at 342 nm, **2** presents the same first two typical emission bands of pyrene but also an extremely more intense signal at 487 nm (Figure 3): the latter is an excimer band related to the stacking interaction of the two pyrenes. In the presence of increasing amounts of both duplex and G4-DNA, such excimer band undergoes a monotonous fluorescence quenching, previously attributed to the increased distance between two pyrenes moieties.[34] Therefore, the fluorescence quenching observed in our experiments
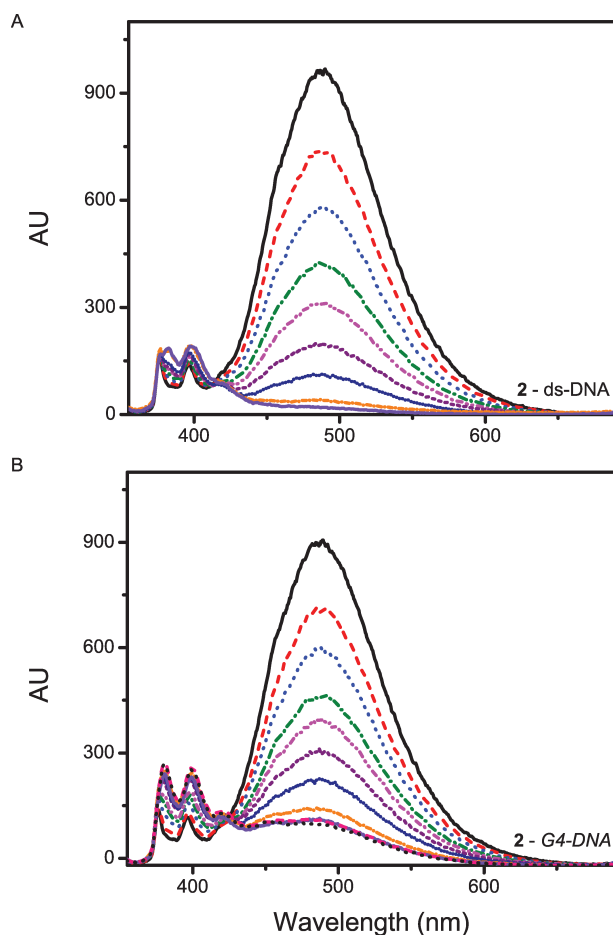


**Figure 3.** Fluorescence emission spectra of **2**-DNA solutions, in 100 mM KCl and 50 mM Tris-HCl buffer: (A) ds-DNA and (B) G4-DNA. A) [**2**] = 5.0 μM, [DNA$_{phosphate}$] = 0.0 – 25.0 μM; (B) [**2**] = 5.0 μM, [G4-DNA] = 0.0 – 3.3 μM.

can be presumably ascribed to the detachment of the two pyrene groups, of the isolated compound **2** in solution, when they become involved in π-stacking interactions with the DNA bases.

## Biological activity

### Compounds 1 and 2 induce cytotoxic effects in breast cancer cells

Encouraged by the results on DNA-binding properties of the title compounds in vitro, we have checked their biological effects on a panel of malignant cell lines, including human colorectal adenocarcinoma, leukemic and breast cancer cells. MTT assay evidenced that both compounds induced cytotoxic effects in all cell lines examined (data not shown). Breast cancer MDA-MB231 and MCF-7 cells were chosen for the study, being representative of a very diffuse and aggressive cancer. Treatment with increasing amounts of **1** and **2** (1.0 - 10 μM) decreased cell viability in a time- and dose-dependent manner (Figure 4A). MDA-MB231 cells were more sensitive to the compounds than MCF-7 cells and compound **1** was more
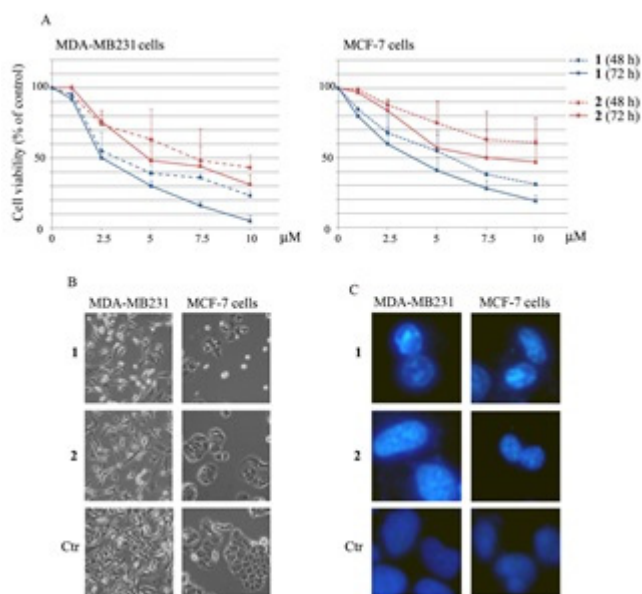
**Figure 4.** Cell proliferation arrest and morphological effects induced by **1** and **2** in MDA-MB231 and MCF-7 cells. (A) Evaluation of cell viability by means of MTT assay. Data, expressed as the percentage of control cells, are means ± S.E. of four independent experiments, involving triplicate assays. Morphological effects induced by treatment for 48 h with 5 μM **1** and 7.5 μM **2**, evaluated by light microscopy (B) and visualization of cell nuclei after staining with Hoechst 33342 and observation under fluorescent microscopy (C). The images are representative of three independent experiments (Original magnification 200X).

effective than **2**. In fact, after 72 h treatment 10 μM **1** reduced MDA-MB231 cell viability by over 90% whereas **2** by about 70%. In MCF-7 cells, instead, cell proliferation was reduced by about 80% and 50%, with **1** and **2**, respectively. The half-maximal inhibitory concentration (IC$_{50}$) of **1** and **2**, evaluated at 48 h of treatment, were 3.3 μM (**1**) and 7.2 μM (**2**) in MDA-MB231 cells, and 5.7 μM (**1**) and >10 μM (**2**) in MCF-7 cells, respectively. For the experiments, when not differently indicated, we employed 5 μM **1** and 7.5 μM **2** in both the cell lines.

Compound-induced effects were confirmed by morphological results. In fact, after treatment for 48 h with **2** a significant reduction in cell number was observed, while in the presence of **1** also rounded and detached cells were found in both the cell lines (Figure 4B). Moreover, Hoechst staining of treated cells evidenced brighter colored and more condensed chromatin than control cells, which appeared with rounded and diffuse stained nuclei (Figure 4C).

A flow cytometry assay was performed in order to determine the percentage of cells in each phase of the cell cycle after treatment with **1** or **2**. The analysis showed that the percentage of cells in the G2/M phase, indicative of a decreased number of dividing cells and related to DNA damage pathways, increased of about 59% and 45% after **1** and **2** treatment respectively, in both cell lines (supplementary Figure S4). Simultaneously, a decrease in the percentage of cells confined in the G0/G1 phase was also observed. These results suggested that the compounds induced cell cycle arrest in G2/M phase

while no evidence of sub-G1 peak, indicative of apoptotic cell death, was found.

### Compounds 1 and 2 induce cellular senescence

To evaluate the effects of both compounds on breast cancer cell proliferation over a relatively long period, subtoxic concentrations (500 nM and 750 nM of **1** and **2**, respectively) were employed to treat MDA-MB231 and MCF-7 cells. Compound **1** induced a rapid arrest of cell growth, and after 14 days cell number reduction in MDA-MB231 cells was such that were no enough cells to reseed (Figure 5A). **2** induced a much
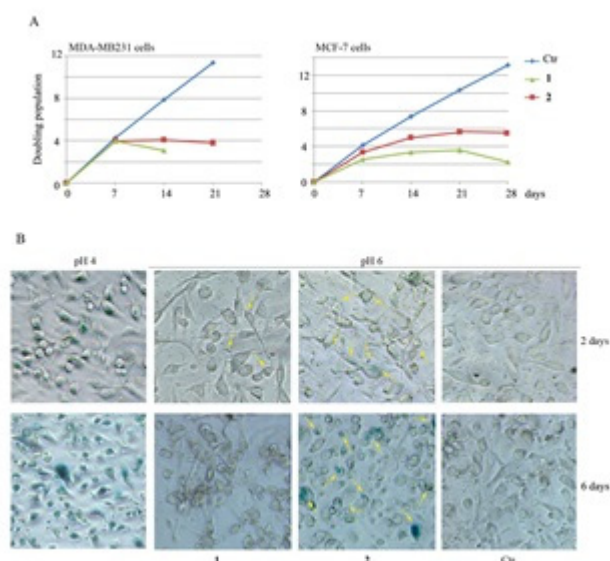


**Figure 5.** Effects of **1** and **2** on long term breast cancer cell proliferation and cell senescence. (A) Cells were treated with 500 nM and 750 nM of **1** and **2**, respectively, counted and passaged at the indicated times. Population doubling values were plotted as a function of days in culture. (B) Increase in the number of senescent MDA-MB231 cells induced by **1** and **2**. After staining, cells were observed under light microscopy. Arrows indicate blue-stained senescent cells. The results reported at pH = 4 represent a positive control of the procedure.

weaker inhibitory effect on cells, being until 28 days the number of cells sufficient to reseeding. These results suggest that the inhibition of cell proliferation induced by **2** might in part be due to cellular senescence following the selective interaction of **2** with telomeric G4-DNA. To confirm the activation of early senescence process, the presence of senescent cells was evaluated by using the β-galattosidase assay.[35]

The analysis showed a time-dependent increase in senescent cells staining-positive for β-galattosidase as compared to control cells in both cell lines. Figure 5B shows the effect observed in MDA-MB231 after treatment for 2 and 6 days with **1** and **2**. The results confirmed the induction of cellular senescence by **2**, possibly caused by the preferential interaction with G4 structures. In the presence of **1**, instead, few cells
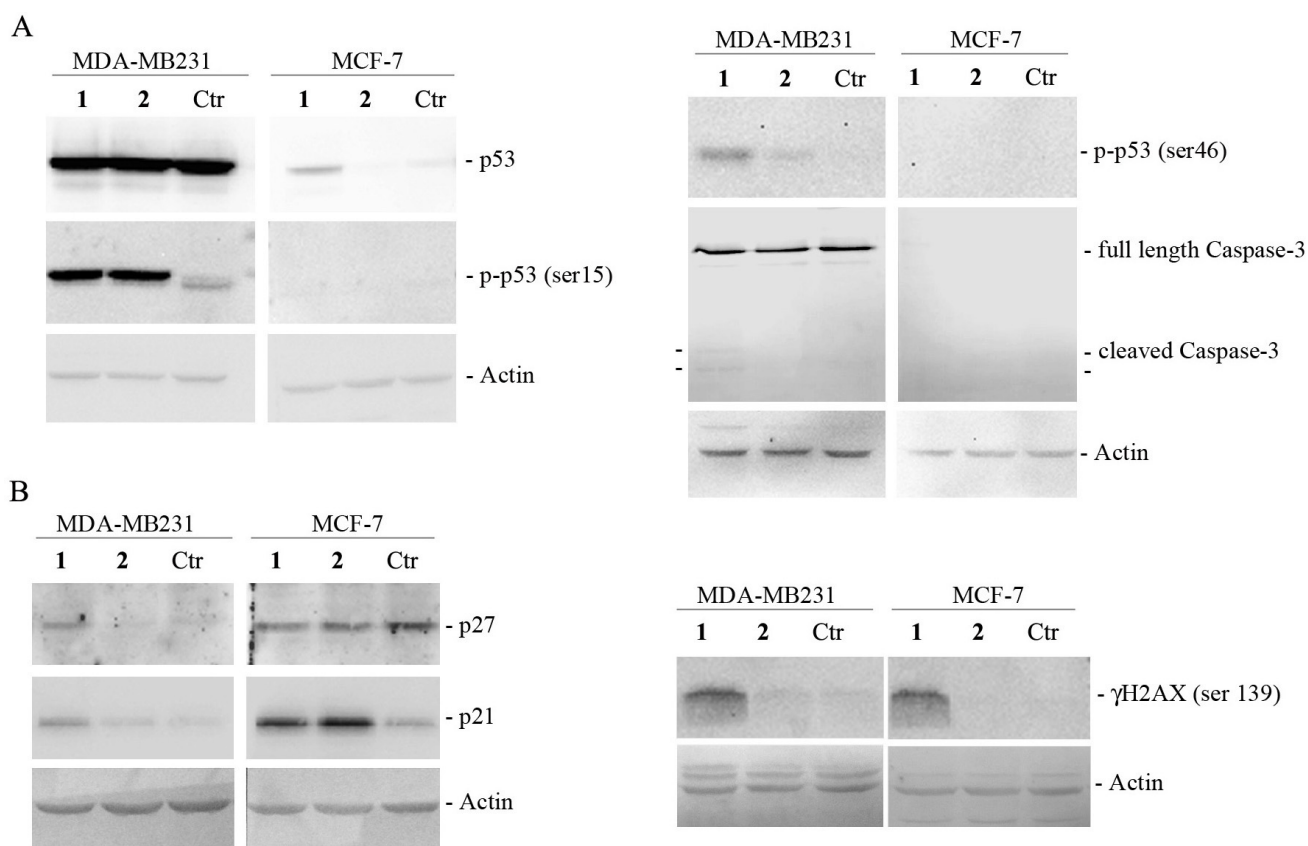
**Figure 6.** Effects of **1** and **2** on the levels of DNA-damage related proteins, p53 and phosphorylated (ser15) and (ser46) p53 and caspase-3 (A) and p27, p21 and γH2AX (B). The results were obtained by immunoblotting. Quantitative densitometric analyses of the results are reported in Supplementary Figure S5.

resulted positive to β-galattosidase after 2 days of treatment while many morphological, death-like changes were detected after 6 days.

### The cytotoxic effects induced by 1 and 2 trigger DNA damage response

The block of cell cycle and the accumulation of cells in G2/M phase are usually consequent to the induction of DNA damage and repair pathway, which can be triggered by telomere target agents.[36] To investigate the biochemical mechanisms underlying to these events, the levels of proteins involved were examined by Western blot assays.

The transcriptional factor p53 is considered a key regulator of cell cycle progression. P53 protein is differently phosphorylated following induction of DNA damage.[37] Therefore, we analysed the status of p53 employing a phospho-Ser15-specific anti-p53 antibody and an antibody that detects p53 regardless of the phosphorylation status. As shown in Figure 6A, in MDA-MB231 cells treated with **1** and **2** for 48 h a marked increase in phospho-p53 (p-p53) was observed while the very high total level of the protein was not modified. Similar results were observed by employing an antibody against Ser46.[38] In particular, a marked increase was observed after treatment with **1**. Since it is well known that MDA-MB231 cells have a mutant

p53, which is characterised by a "gain of function",[39] phospho-p53 increase can be interpreted as an attempt of response by the cells to DNA damage, consequent to the interaction of the derivatives with G4 and/or duplex DNA. Interestingly, the analysis of the level of caspase-3, the main executioner apoptotic protease, showed the appearance of the cleaved active forms in **1**-treated MDA-MB231 cells, indicating that an apoptotic pathway is activated in these cells, even if this is not accompanied to the activation of specific endonucleases. Differently, in MCF-7 cells the low basal level of p53 wild type increased after treatment with **1**, but this effect was not accompanied by the increase in the phosphorylated forms. As expected, no band corresponding to caspase-3 was detected in MCF-7, being these cells caspase-3 deficient.

Additionally, p21 and p27, two key downstream regulators of cell cycle arrest,[40] were also increased in MDA-MB231 cells after treatment with **1** and **2**, being **1** the most active compound (Figure 6B). This increase could be related to the specific increase in phospho-p53 observed after treatment with **1**. The analysis in MCF-7 cells showed that p27 levels were not modified by treatment with **1** and **2**, while p21 showed a very marked increase after treatment, which was, most probably, a p53-independent event.

Finally, we analysed the level of histone variant H2AX. This protein plays an important role in DNA-damage response and

its phosphorylation and activation is required for the assembly of repair proteins and the arrest of cell cycle progression.[41] As shown in Figure 6B, in both cell lines **1** induced a remarkable increase in the level of phosphorylated γH2AX after 48 h treatment, while **2** was almost ineffective. Altogether, the analysis of the protein levels supports the hypothesis that **1**, being able to interact with both ds-DNA and G4-DNA structures, triggers death process phospho-p53, p21 and γH2AX- mediated, while **2**, mainly binding G4 structures, halts telomeric lengthening, which is a very important step for cancerogenesis.

**Molecular modeling**

To interpret the results of the DNA-binding and biological studies, providing atomic level models of the title compounds-DNA binding complexes, molecular modeling investigations have been performed. In particular, the results from molecular dynamics simulations show that the DNA binding of **1** and **2** is qualitatively similar but quantitatively different.

Concerning the binding with ds-DNA, as expected, **1** is a typical DNA-intercalator (Figure 7A). As shown in the RMSD
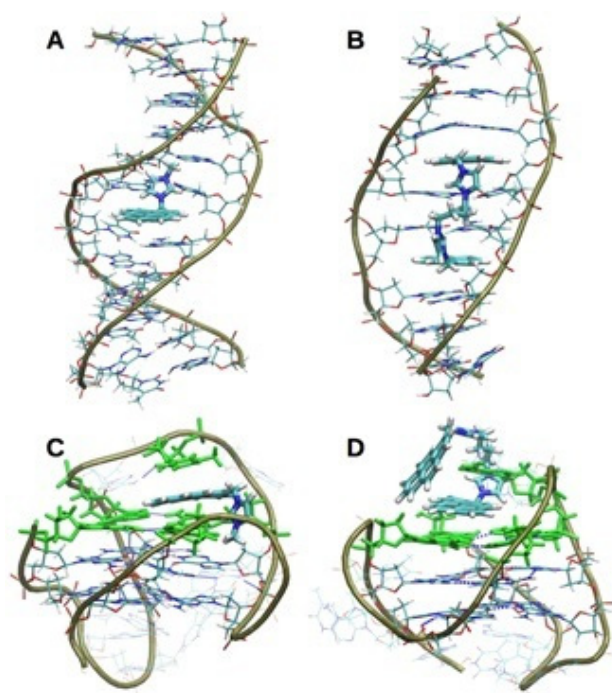


**Figure 7.** Representative snapshots extracted at the equilibrium of the MD simulations, showing the preferential binding modes of **1** and **2** with ds- and G4-DNA. A) **1** intercalated in ds-DNA; B) **2** bis-intercalated in ds-DNA; C) **1** top-stacked to the 3' quartert (green) of G4-DNA with a further stacking interaction with A13 (green) from the TAA loop above; D) one pyrene of **2** top-stacked with the 3' quartet (green) of G4-DNA, involved also in a stacking interaction with T12 (green), while the second pyrene group is involved in an edge-to-face interaction with T12.

plot (supplementary Figure S6), during 200 ns of MD simulation the binding pocket of the double helix adapts to the intercalator, with average oscillations of about 2.5 Å around an equilibrium structure.

Compound **2** binds ds-DNA preferentially through bis-intercalation of the two pyrene moieties, on two intercalation sites axially separated by two base-pairs (Figure 7B). At the equilibrium, average oscillations of about 2 Å are observed in the relative RMSD plot (supplementary Figure S7). It is worth pointing out that molecular docking provided starting structures in which **2** was bound to both the major and minor grooves of DNA. However, such models were not stable during the MD simulations, which are always prone to intercalation, inducing strong distortion of the double helix.

Concerning the binding with G4-DNA, again as expected, Figure 7C shows that **1** mainly interacts through top-stacking with the G-tetrad below the TTA loop made by the T11, T12 and A13 bases. Moreover, a further stabilising stacking interaction with T12 occurs.

The binding of **2** with G4-DNA mainly occurs through top-stacking with the same G-tetrad. However, the presence of the second pyrene ring and of a dicationic charge makes this interaction stronger than that shown by compound **1**. In fact, the top-stacking interaction of one pyrene group is further assisted by i) a stacking interaction with T12 of the TTA loop and ii) an edge-to-face interaction between T12 and the second pyrene ring (Figure 7D). Also in this case, the docking calculations provided a starting structure in which the self-stacked conformation of **2** was in the largest groove of the G4-DNA. However, this interaction was not stable during the MD simulation and stacking interactions between the pyrene rings and loop bases were preferred. Overall, the results obtained point out that molecular docking investigation alone cannot provide a reliable support for the structural interpretation of experimental spectroscopic data.

The RMSD plots of all the binding complexes with G4-DNA (supplementary Figures S8 and S9) show that they are more rigid than the intercalation complexes with duplex-DNA.

Interestingly, the results of the MD simulations, concerning the binding of **2** with both duplex and quadruplex DNA, provide a useful interpretation of the fluorescence quenching shown in Figure 3. In fact, in both cases the binding involves an increase of the relative distance between the two pyrene moieties, responsible for the decrease of the excimer emission. However, after binding with G4-DNA and duplex-DNA, the distance between the two pyrene moieties is shorter and longer, respectively. This result provides an explanation of the non-complete fluorescence quenching observed in Figure 3B.

## Conclusions

DNA-binding investigations, with the help of molecular modeling, provided structure-activity relationships that support the differences between the biological activities of **1** and **2.** The isolated pyrene-imidazolium, **1**, binds to G4-DNA with a $K_b$ only one order of magnitude larger than that related to the binding to ds-DNA ($1.8 \times 10^5$ M$^{-1}$ vs. $1.3 \times 10^4$ M$^{-1}$), while the presence

of a $C_4$ linker induces a preferential affinity of **2** toward G4-DNA of two orders of magnitude compared to ds-DNA ($2.1 \times 10^6$ *vs.* $3.8 \times 10^4$ M$^{-1}$). Moreover, senescence induction by **2** is indicative of an interaction with telomeric DNA-sequences. MD simulations suggest that the stronger G4-DNA binding of **2** is a consequence of the occurrence of additional edge-to-face interactions with the T12 base of the TTA loop connecting the G10 and G14 bases of the terminal G-quartet. In conclusion, the interpretation of the DNA-binding studies, supported by molecular modeling, provided indications on the design of new compounds that will be performed in forthcoming studies to improve G4-DNA selectivity and to reduce ds-DNA affinity, maintaining water solubility.

## Supporting Information Summary Paragraph

The Experimental Section, additional UV-vis, CD, Fluorescence, melting profiles, flow-cytometry, quantitative densitometric analysis and RMSD plots are reported in the Supporting Information.

## *Acknowledgements*

[1] Y. Du, J. Huang, X. Weng, X. Zhou, *Curr. Med. Chem.* **2010**, *17*, 173—189.
[2] L. H. Hurley, *Nat. Rev. Cancer* **2002**, *2*, 188–200.
[3] M. J. Hannon, *Chem. Soc. Rev.* **2007**, *36*, 280—295.
[4] J. Lavrado, S. A. Ohnmacht, I. Correia, C. Leitão, S. Pisco, M. Gunaratnam, R. Moreira, S. Neidle, D. J. V. A. dos Santos, A. Paulo, *ChemMedChem* **2015**, *10*, 836—849.
[5] A. A. Almaqwashi, T. Paramanathan, I. Rouzina, M. C. Williams, *Nucleic Acids Res.* **2016**, *44*, 3971—3988.
[6] W. A. Denny, *Curr. Med. Chem.* **2002**, *9*, 1655—1665.
[7] R. Bonsignore, A. Terenzi, A. Spinello, A. Martorana, A. Lauria, A. M. Almerico, B. K. Keppler, G. Barone, *J. Inorg. Biochem.* **2016**, *161*, 115—121.
[8] A.-M. Meredith, C. R. Dass, *J. Pharm. Pharmacol.* **2016**, *68*, 729—741.
[9] A. C. Komor, J. K. Barton, *J. Am. Chem. Soc.* **2014**, *136*, 14160–14172.
[10] A. Terenzi, L. Tomasello, A. Spinello, G. Bruno, C. Giordano, G. Barone, *J. Inorg. Biochem.* **2012**, *117*, 103—110.
[11] H. N. Kim, E.-H. Lee, Z. Xu, H.-E. Kim, H.-S. Lee, J.-H. Lee, J. Yoon, *Biomaterials* **2012**, *33*, 2282—2288.
[12] J. L. Huppert, *Chem. Soc. Rev.* **2008**, *37*, 1375—1384.
[13] G. Biffi, D. Tannahill, J. McCafferty, S. Balasubramanian, *Nat. Chem.* **2013**, *5*, 182—186.
[14] D. Rhodes, H. J. Lipps, *Nucleic Acids Res.* **2015**, *43*, 8627—8637.
[15] S. Neidle, *J. Med. Chem.* **2016**, *59*, 5987—6011.
[16] R. Rodriguez, S. Müller, J. A. Yeoman, C. Trentesaux, J.-F. Riou, S. Balasubramanian, *J. Am. Chem. Soc.* **2008**, *130*, 15758—15759.
[17] S. Neidle, G. Parkinson, *Nat. Rev. Drug Discov.* **2002**, *1*, 383—393.
[18] S. N. Georgiades, N. H. Abd Karim, K. Suntharalingam, R. Vilar, *Angew. Chem. Int. Ed.* **2010**, *49*, 4020—4034.
[19] D. Drygin, A. Siddiqui-Jain, S. O'Brien, M. Schwaebe, A. Lin, J. Bliesath, C. B. Ho, C. Proffitt, K. Trent, J. P. Whitten, et al., *Cancer Res.* **2009**, *69*, 7653—7661.
[20] Z. Xu, N. J. Singh, J. Lim, J. Pan, H. N. Kim, S. Park, K. S. Kim, J. Yoon, *J. Am. Chem. Soc.* **2009**, *131*, 15528—15533.
[21] S. J. Moon, S. H. Park, J. Jaworski, J. H. Jung, *Chem. Commun.* **2013**, *49*, 11698—11700.
[22] S. Wang, L. Ding, J. Fan, Z. Wang, Y. Fang, *ACS Appl. Mater. Interfaces* **2014**, *6*, 16156—16165.
[23] D. L. Ang, B. W. J. Harper, L. Cubo, O. Mendoza, R. Vilar, J. Aldrich-Wright, *Chem. - Eur. J.* **2016**, *22*, 2317—2325.
[24] P. Yang, A. De Cian, M.-P. Teulade-Fichou, J.-L. Mergny, D. Monchaud, *Angew. Chem. Int. Ed.* **2009**, *48*, 2188—2191.
[25] M. Tera, T. Hirokawa, S. Okabe, K. Sugahara, H. Seimiya, K. Shimamoto, *Chem. – Eur. J.* **2015**, *21*, 14519—14528.
[26] H. Bertrand, S. Bombard, D. Monchaud, M.-P. Teulade-Fichou, *J. Biol. Inorg. Chem. JBIC Publ. Soc. Biol. Inorg. Chem.* **2007**, *12*, 1003—1014.
[27] A. E. Hargrove, Z. Zhong, J. L. Sessler, E. V. Anslyn, *New J. Chem.* **2010**, *34*, 348.
[28] P. Thordarson, *Chem Soc Rev* **2011**, *40*, 1305–1323.
[29] R. Lying, A. Rodger, B. Nordén, *Biopolymers* **1991**, *31*, 1709—1720.
[30] A. Terenzi, R. Bonsignore, A. Spinello, C. Gentile, A. Martorana, C. Ducani, B. Högberg, A. M. Almerico, A. Lauria, G. Barone, *RSC Adv.* **2014**, *4*, 33245—33256.
[31] N. Zhang, A. T. Phan, D. J. Patel, *J. Am. Chem. Soc.* **2005**, *127*, 17277—17285.
[32] Y. Xu, Y. Noguchi, H. Sugiyama, *Bioorg. Med. Chem.* **2006**, *14*, 5584—5591.
[33] S. Ghosh, A. Al Masum, A. Ganguly, M. A. Alam, M. M. Islam, N. Guchhait, *RSC Adv.* **2016**, *6*, 93335—93342.
[34] G. K. Bains, S. H. Kim, E. J. Sorin, V. Narayanaswami, *Biochemistry (Mosc.)* **2012**, *51*, 6207—6219.
[35] F.-C. Huang, C.-C. Chang, J.-M. Wang, T.-C. Chang, J.-J. Lin, *Br. J. Pharmacol.* **2012**, *167*, 393—406.
[36] M. P. Longhese, *Genes Dev.* **2008**, *22*, 125—140.
[37] H. Zhao, F. Traganos, Z. Darzynkiewicz, *Cell Cycle* **2008**, *7*, 3048—3055.
[38] M. Kodama, C. Otsubo, T. Hirota, J. Yokota, Y. Enari, Y. Taya, *Mol. Cell. Biol.* **2010**, *30*, 1620–1633.
[39] N. Shtraizent, H. Matsui, A. Polotskaia, J. Bargonetti, *Int. J. Environ. Res. Public. Health* **2016**, *13*, DOI 10.3390/ijerph13010022.
[40] D. A. Foster, P. Yellen, L. Xu, M. Saqcena, *Genes Cancer* **2010**, *1*, 1124—1131.
[41] C.-Y. Wu, H.-Y. Kang, W.-L. Yang, J. Wu, Y. S. Jeong, J. Wang, C.-H. Chan, S.-W. Lee, X. Zhang, B. Lamothe, et al., *J. Biol. Chem.* **2011**, *286*, 30806—30815.